Journal of Computational Physics 228 (2009) 5251–5261

Contents lists available at ScienceDirect

Journal of Computational Physics

journal homepage: www.elsevier.com/locate/jcp

Virtual experiments: Combining realistic neutron scattering instrument and sample simulations

E. Farhi [a,*], V. Hugouvieux [b], M.R. Johnson [a], W. Kob [c]

[a] Institut Laue Langevin, BP 156, 38042 Grenoble Cedex 9, France
[b] INRA, UR1268 Biopolymères Interactions Assemblages, F-44300 Nantes, France
[c] Laboratoire des Colloïdes, Verres et Nanomatériaux, Université Montpellier II, place E. Bataillon, 34095 Montpellier Cedex 5, France

ARTICLE INFO

Article history:
Received 19 June 2008
Received in revised form 26 March 2009
Accepted 8 April 2009
Available online 18 April 2009

PACS:
02.70.Ns
02.70.Uu
25.40.Dn
25.40.Fq
29.30.Hs
31.15.-p
47.11.Mn
61.05.fg
61.20.Ja
61.25.Mv
78.70.Nx

Keywords:
Neutron scattering
Molecular dynamics
Liquids
Instrument simulation
Monte Carlo simulation
Multiple scattering

ABSTRACT

A new sample component is presented for the Monte Carlo, ray-tracing program, *McStas*, which is widely used to simulate neutron scattering instruments. The new component allows the sample to be described by its material dynamic structure factor, which is separated into coherent and incoherent contributions. The effects of absorption and multiple scattering are treated and results from simulations and previous experiments are compared.

The sample component can also be used to treat any scattering material which may be close to the sample and therefore contaminates the total, measured signal.

1. Introduction

Neutron scattering provides a large variety of instruments to probe structure and dynamics of condensed matter. However, the technique is flux limited, which motivates continuous efforts to improve both the flux and the overall efficiency of the instruments. Therefore both analytical and numerical methods are used in order to determine optimal instrument configurations.

* Corresponding author. Tel.: +33 4 76 20 71 35; fax: +33 4 76 20 76 48.
E-mail address: farhi@ill.fr (E. Farhi).

0021-9991/$ - see front matter © 2009 Elsevier Inc. All rights reserved.
doi:10.1016/j.jcp.2009.04.006

For simple neutron beam configurations, analytical models are available to describe the different neutron optics elements of the instruments, which modify the characteristics of the beam (e.g. divergence, wavelength spread, spatial and time distributions). This approach is valid for individual elements such as guides [1,2], choppers [3,4], Fermi choppers [5,6], velocity selectors [7], monochromators [8–11], and detectors [12–14]. In the case of a limited number of optical elements, the so-called acceptance diagram theory [2,15,16] may be used, within which the neutron beam distributions are considered to be homogeneous, triangular or Gaussian. However, real neutron instruments are composed of a large number of optical elements, and this brings additional complexity by introducing strong correlations between neutron beam parameters like divergence and position – which is the basis of the acceptance diagram method – but also wavelength and time. The usual analytical methods, such as phase-space theory, then reach their limit of validity in the description of the resulting effects.

In order to cope with this difficulty, the simulation of neutron spectrometers may be performed using Monte Carlo methods (for a general review, see Ref. [17]), which are commonly used for the description of microscopic physical processes such as absorption, scattering or reflection. Integrating these events over the neutron trajectories results in an estimation of measurable quantities characterizing the neutron instrument. Moreover, using importance sampling reduces the computation time and gives better accuracy. Early implementations of the Monte Carlo method for neutron instruments used *home-made* computer programs (see [18,19]) but, more recently, general packages have been designed, providing models for most optical components of neutron spectrometers. The most widely-used packages are NISP [20], ResTrax [21], McStas [22], Vitess [23], and IDEAS [24], which allow a wide range of neutron scattering instruments to be simulated. The neutron ray-tracing Monte Carlo method has been used widely for guide studies [15,25,26], instrument optimisation and design [27–29]. Since Monte Carlo ray-tracing gives accurate estimates for the flux and resolution, it enables optimum parameter sets for the instrument to be determined, which is not always possible with classical analytical methods. In addition, as for any instrument, in certain experiment configurations, the experimental signal may be contaminated due to various contributions to the total signal coming either from the instrument or from the sample such as background, coherent and incoherent scattering, self-shielding and multiple scattering.

Some of these questions may be tackled directly with Monte Carlo neutron scattering instrument simulations but others depend intrinsically on the sample. Indeed the experimental signal is the convolution of the instrument response and the signal due to the interaction between neutrons and the sample (structure and dynamics). Separating instrument and sample contributions requires both to be known in detail. As a consequence, the concept of virtual experiments [30], that is simulations including accurate models for both instruments and samples, has recently become a logical and important extension of Monte Carlo neutron scattering instrument simulations. For instance, for the multiple scattering contribution, no experimental method makes it possible to accurately measure this contribution, even though it can become significant at low q momentum transfers, for example, below the first diffraction maximum in liquids and glasses, where the single scattering coherent signal is weak in most materials. This is why attempts have been made to reduce the multiple scattering contribution by partitioning the sample with absorbing layers, as in [31]. However, this is not always applicable thus making the simulation approach very valuable.

Many methods and approximations have been developed to quantify these contributions and, for example, analytical formulae exist that can be applied for correcting multiple scattering [32]. However, these methods remain limited in their capability to handle strongly cross correlated neutron parameter states, which originate from, e.g. complex instrument and sample geometry descriptions. A number of previous Monte Carlo codes [33–36] have been designed to evaluate single and multiple scattering, absorption, self-absorption and transmission factors. However, they are often limited regarding, e.g. the instrument geometry, the sample environment and shape, or the type of experiment (diffraction, time-of-flight).

This paper presents the component *Isotropic_Sqw* in the *McStas* code [22]. It allows the sample scattering function $S(q,\omega)$, where q and ω are the wavevector and energy transfers, to be included in a Monte Carlo neutron scattering instrument simulation. This implies that both elastic and inelastic scattering are taken into account, for the coherent and incoherent processes. The object of the study is to demonstrate that complex instrument descriptions can be coupled to sample simulations in order to produce virtual experiment results that compare with real measurements.

In the next section, the general principle of sample simulations, dedicated to the global simulation of neutron scattering experiments, is explained. In Section 3 we compare a virtual experiment on liquid Rb with the direct analysis of the corresponding experimental data and we focus on the possibilities for handling multiple scattering in order to demonstrate the usefulness of such a numerical approach for the analysis of experimental data. While the rubidium work does not reveal a particular high level of multiple scattering, we regard the work of Copley [31] as a reference in this context. Finally we discuss the results and give some perspectives of the present work.

2. Sample simulation for virtual neutron scattering experiments

With a view to performing virtual neutron scattering experiments, a new sample component has been developed for the *McStas* package [22] in order to simulate neutron scattering from any isotropic material such as liquids, glasses (amorphous systems), polymers and powders (currently, mono-crystals cannot be handled by this component). The component *Isotropic_Sqw* treats coherent and incoherent neutron scattering and may be used to model most materials, including sample environments with concentric geometries. The method presented here for handling neutron interaction with isotropic materials is similar in many respects to the earlier MSC [33], Discus [34] and MSCAT [35] methods, but the implementation presented here is part of a more general treatment of a sample in an instrument.

In the following, we consider an isotropic medium irradiated with a cold or thermal neutron beam. We ignore the possible thermal fission events and assume that the incoming neutron energy does not correspond to a Breit–Wigner resonance in the material. Furthermore, we do not take into account quantum effects in the material, nor refraction and primary extinction.

The justification of using the dynamic structure factor $S(q,\omega)$ for the description of the scattering events is given by following Squires [37]. The experimental counterpart of the scattering law $S(q,\omega)$ is the neutron double differential scattering cross section for both coherent and incoherent processes:

$$\frac{d^2\sigma}{d\Omega\, dE_f} = \frac{\sigma}{4\pi}\frac{k_f}{k_i} NS(q,\omega), \tag{1}$$

which describes the number of neutrons scattered per unit solid angle $d\Omega$ and per unit final energy dE_f. In this equation, $N=\rho V$ is the number of atoms in the scattering volume V with atomic number density ρ, E_f, E_i, k_f, k_i are the kinetic energies and wavevectors of final and initial states respectively, σ is the bound atom scattering cross section, Ω is the solid angle and q,ω are the wavevector and energy transfer at the sample. In practice, the double differential cross section is a linear combination of the coherent and incoherent parts of the dynamic structure factor as:

$$\sigma S(q,\omega) = \sigma_{coh} S_{coh}(q,\omega) + \sigma_{inc} S_{inc}(q,\omega), \tag{2}$$

where σ_{coh} (resp. σ_{inc}) is the bound atom coherent (resp. incoherent) scattering cross section. Consequently the structure and dynamics of isotropic samples can be characterised by the quantity $\sigma S(q,\omega)$, which completely determines the interaction between neutrons and the sample and therefore can be used as a probability distribution of ω-energy and q-momentum transfers.

We consider a neutron with a given position and incident wavevector k_i and energy E_i. In view of computing the interaction between a neutron and a material of given volume and shape, the first step consists in determining the propagation path length in the material by geometrical intersections between the neutron trajectory and the sample volume. Along this path, the neutron may either interact with atoms of the sample, through absorption or scattering, or be transmitted without interaction with the material and exit the sample.

The probability of such an interaction is governed by the energy dependent total cross section σ_{tot} accounting for both scattering and absorption, defined as:

$$\sigma_{tot}(E_i) = \sigma_{abs}(E_i) + \sigma_s(E_i). \tag{3}$$

In this expression, the cross sections σ_{abs} and σ_s reflect the effective interaction surface for absorption and scattering respectively between a neutron of energy E_i and an atom of the material.

Therefore, before determining what happens to the neutron, we have to compute the different contributions to the total cross section, namely $\sigma_{abs}(E_i)$ and $\sigma_s(E_i)$. These quantities actually govern the ratio of absorption to scattering in the material for a given incident energy E_i.

2.1. Cross sections

Except for a few materials with absorption resonances in the cold-thermal energy range, the absorption cross section for an incoming neutron of velocity $v_i=\sqrt{2E_i/m}$ (in m/s), where m is the neutron mass, is computed as

$$\sigma_{abs}(E_i) = \sigma_{abs}^{2200}\frac{2200}{\sqrt{2E_i/m}}, \tag{4}$$

where σ_{abs}^{2200} is the absorption cross section for a neutron with $v_i = 2200$ m/s and is obtained from the literature [38].

Following Sears [32], the total scattering cross section for incoming neutrons with initial energy E_i is

$$\sigma_s(E_i) = \int\int \frac{d^2\sigma}{d\Omega\, dE_f}\, d\Omega\, dE_f = \frac{N\sigma}{4\pi}\int\int \frac{k_f}{k_i} S(q,\omega) d\Omega\, dE_f, \tag{5}$$

where the integration runs over the entire space and all final neutron energies. As the dynamic structure factor is defined in the (q,ω) space, the integration requires a variable change. Using the momentum conservation law $\vec{q}=\vec{k}_i-\vec{k}_f$ and the solid angle relation $\Omega = 2\pi(1-\cos\theta)$, where θ is the solid angle opening, we obtain:

$$\sigma_s(E_i) = N\int\int \frac{\sigma S(q,\omega) q}{2k_i^2}\, dq\, d\omega. \tag{6}$$

This integration runs over the whole accessible (q,ω) dynamical range for each incoming neutron. The dynamic structure factor needs only to be known for $\omega>0$ (anti-Stokes processes, neutron gains energy), as

$$S(q,-\omega) = e^{\hbar\omega/k_BT} S(q,\omega). \tag{7}$$

This correction will be applied in Section 2.5, and we now consider that $\omega>0$. In practice, the knowledge of the dynamic structure factor is defined over a limited area with $q\in[q_{min},q_{max}]$ and $\omega\in[\omega_{min},\omega_{max}]$ which is constrained by the method for obtaining $S(q,\omega)$, i.e. from previous experiments, molecular dynamics simulations, and analytical models. It is desirable that this area be as large as possible, starting from 0 for both ranges. If we use $\omega_{min}\to 0$, $q_{min}\to 0, \hbar\omega_{max} > 4E_i$ and $q_{max} > 2k_i$,

we completely describe all scattering processes for incoming neutrons with wavevector k_i [33]. This means that in order to correctly estimate the total intensity and multiple scattering, the knowledge of $S(q,\omega)$ must be wider (at least twice in q, as stated previously) than the measurable range in the corresponding experiment. As a side effect, a self-consistent iterative method for finding the true scattering law from the measurement itself is not theoretically feasible, except for providing crude approximations. However, the measured dynamic structure factor may be used to estimate the multiple scattering for a further measurement using at least twice longer wavelength neutrons. Extrapolating the scattering law beyond the accessible measurement range might improve substantially the applicability of the method, but such a discussion is beyond the scope of this paper.

Consequently, limiting the q integration in Eq. (6) to the maximum momentum transfer for elastic processes $2k_i$, we write the total scattering cross section as

$$\sigma_s(E_i) \simeq \frac{N}{2k_i^2}\int_0^{2k_i} q\sigma S(q)\,dq. \tag{8}$$

Using Eq. (2), it is possible to define similar expressions for the coherent and incoherent terms $\sigma_{coh}(E_i)$ and $\sigma_{inc}(E_i)$ respectively. These integrated cross sections are usually quite different from the tabulated values [38] since the latter are bound scattering cross sections.

Once the absorption and scattering cross sections are known, we can compute transmission, absorption and scattering event probabilities.

2.2. Transmission

The transmission probability follows an exponential decay law accounting for the total cross section. The neutron trajectory intersection with the sample geometry provides the total path length in the sample d_{exit} to the exit. Defining the linear attenuation $\mu(E_i) = \rho\sigma_{tot}(E_i)$, the probability that the neutron event is transmitted along path d_{exit} is $e^{-\mu(E_i)d_{exit}}$. Consequently, we determine if the neutron interacts with the sample by drawing a random number ξ_t in the range [0, 1]. Note that whenever we refer to random numbers, a uniform generator is used [39]. In the following, we introduce the neutron Monte-Carlo statistical weight, which represents the probability of a given neutron event to participate in the total intensity at a given position in the course of the simulation.

In case of transmission, the neutron leaves the sample. In previous Monte Carlo codes such as MSC [33], DISCUSS [34] and MSCAT [35], each exiting neutron event is forced to scatter to the detector area in order to improve the sample scattering simulation statistics and reduce the computing time. This method requires to focus the measurable energy and momentum transfers for the last scattering event in the sample towards the detectable area, so that the choice of the scattering excitation actually requires a more complex sampling mechanism from the dynamic structure factor. The corresponding instrument model is limited to a neutron event source, a sample and a detector. In the current implementation, it is equally possible to 'force' neutron events to scatter (and possibly reach the detector) by applying a correction factor $\pi_0 = 1 - e^{-\mu(E_i)d_{exit}}$ to the neutron statistical weight, in which case there is no need to cast the random number ξ_t for transmission probability. However, the *McStas* instrument model is often built from a large sequence of components [22]. Even though the instrument description starts as well with a neutron event source, more than one sample may be encountered in the course of the neutron propagation and multiple detectors may be positioned anywhere in space, as well as other instrument components (e.g. filters, mechanical parts, samples, shields, radiation protections). This implies that, in this case, neutron events scattered from a sample volume should not focus to a single area. Indeed, transmitted events may reach other scattering materials and it is not desirable to force all neutron events to scatter. In this case, the correction factor π_0 is therefore not applied, and neutron events can be transmitted through the sample volume. The simulation efficiency for the scattering is certainly lower, but enables much more complex arrangements, such as concentric sample environments, magnets and monochromator mechanical parts, and neutron filters, to be modelled.

2.3. Scattering and absorption

If the neutron is not transmitted, it may be either absorbed or scattered. In order to avoid loosing neutron events through absorption, we consider that all interacting neutron events scatter and the neutron statistical weight is multiplied by a factor

$$\pi_1 = \frac{\sigma_s(E_i)}{\sigma_{tot}(E_i)} \tag{9}$$

to account for the fraction of absorbed neutrons along the path. Additionally, the type of interaction (coherent or incoherent) is chosen randomly with fractions $\sigma_{coh}(E_i)/\sigma_s(E_i))$ and $\sigma_{inc}(E_i)/\sigma_s(E_i)$.

Then we select a scattering position along the path, taking into account the secondary extinction and absorption probability. In this process, the neutron is considered to be a particle or an attenuated wave. The position of the neutron scattering event along the neutron trajectory length d_{exit} is determined by [19,34]

$$d_s = -\frac{1}{\mu(E_i)}\ln(1 - \xi_d[1 - e^{-\mu(E_i)d_{exit}}]), \tag{10}$$

where ξ_d is a random number in [0, 1]. This expression takes into account secondary extinction, originating from the decrease of the beam intensity through the sample (self-shielding).

2.4. Choice of the energy and momentum transfers

Once a scattering position has been assigned, the neutron interacts with a material excitation. Here we turn to the wave description of the neutron, which interacts with the whole sample volume. The distribution of excitations, which determines their relative intensity in the scattered beam, is simply the dynamic structure factor – or scattering law – $S(q,\omega)$. We build probability distributions from the scattering law in order to improve the efficiency of the method by favoring the (q,ω) regions with larger $S(q,\omega)$ values.

The choice of the (q,ω) wavevector-energy transfer pair could be done randomly, as in the first event of the second order scattering evaluation in DISCUS [34], but it is somewhat inefficient except for materials showing a broad quasi-elastic signal. As the scattering originates from structural peaks and excitations in the material $S(q,\omega)$, it is usual [35] to adopt an importance sampling scheme by focusing the (q,ω) choice to areas where the intensity of $S(q,\omega)$ is high. In practice, this means that the neutron event should scatter preferably on, for example, Bragg peaks, quasielastic contributions and phonons.

The main idea to implement the scattering from $S(q,\omega)$ is to cast two consecutive Monte Carlo choices, using probability distribution built uniformly from the dynamic structure factor. We define first the probability $P_\omega(\omega)d\omega$ as the *unweighted* fraction of modes whose energy lies between ω and $\omega + d\omega$

$$P_\omega(\omega) = \frac{\int_0^{q_{max}} S(q,\omega)\,dq}{|S|}, \tag{11}$$

where $|S| = \int\int S(q,\omega)\,dq\,d\omega$ is the norm of $S(q,\omega)$ in the available dynamical range $q \in [q_{min}, q_{max}]$ and $\omega \in [\omega_{min}, \omega_{max}]$. The probability P_ω is normalised to unity, $\int_{\omega_{min}}^{\omega_{max}} P_\omega(\omega')\,d\omega' = 1$, and is a probability distribution of mode energies in the material. The energy transfer ω for scattering is determined by casting a random number $\xi_\omega \in [0,1]$ and solving the equation

$$\xi_\omega = \int_{\omega_{min}}^{\omega} P_\omega(\omega')\,d\omega'. \tag{12}$$

Similarly, in order to focus the wavevector transfer choice, we define the probability distribution of wavevector $P_q(q \mid \omega)\,d\omega\,dq$ for the selected energy transfer lying between ω and $\omega + d\omega$

$$P_q(q \mid \omega) = \frac{S(q,\omega)}{S(q)}, \tag{13}$$

from which we choose randomly a wavevector transfer q, knowing the energy transfer ω. As for the energy transfer, we cast a random number $\xi_q \in [0,1]$ and determine the corresponding wavevector transfer q which solves the equation

$$\xi_q = \int_{q_{min}}^{q} P_q(q' \mid \omega)\,dq'. \tag{14}$$

The right members in Eqs. (12) and (14) are monotonically increasing primitives of P_ω and P_q, which only depend on the dynamical structure factor S. This procedure ensures that the energy and wavevector choice is performed on a uniform (q,ω) space but statistically focuses scattering events where the scattering function is higher.

Then a selection between energy gain and loss is performed with the detailed balance ratio $e^{-\hbar\omega/k_BT}$. In the case of Stokes processes, the neutron can not loose more than its own energy to the sample dynamics, so that $\hbar\omega < E_i$. This condition breaks the symmetry between up-scattering and down-scattering.

2.5. Solving selection rules and choosing the scattered wavevector

The next step is to check that the conservation laws

$$\hbar\omega = E_i - E_f = \frac{\hbar^2}{2m}(k_i^2 - k_f^2), \tag{15}$$

$$\vec{q} = \vec{k}_i - \vec{k}_f \tag{16}$$

can be satisfied. These conditions are closely related to the method for selecting the outgoing wavevector direction.

When the final wavevector has to be computed, the quantities $\vec{k}_i, \hbar\omega$ and $q = |\vec{q}|$ are known. We solve the energy conservation law Eq. (15) and we select randomly k_f as one of the two roots. The scattering angle θ from the initial k_i direction is determined from the momentum conservation law $\cos(\theta) = (k_i^2 + k_f^2 - q^2)/(2k_ik_f)$, which defines a scattering cone. We then choose randomly a direction on the cone. If the selection rules can not be verified (namely $|\cos(\theta)| > 1$), a new (q,ω) random choice is performed (see Section 2.4). It might appear inefficient to select the energy and momentum transfers first and check the selection rules afterwards. However, in practice, the number of iterations to actually scatter on a high probability process and satisfy these rules is limited, usually below 10. Moreover, as these two steps are simple, the whole process requires a limited number of computer operations.

Once the scattering probability and position, the energy and momentum transfers and the neutron momentum after scattering have all been defined, the whole process is iterated until the neutron is transmitted and exits the sample volume.

2.6. Schematic neutron-matter interaction implementation

The processing of the interactions between neutrons and sample can be summarized as follows:

(1) Compute the propagation path length in the material by geometrical intersections between the neutron trajectory and the sample volume.
(2) Evaluate the total cross section from the integration of the scattering law over the accessible dynamical range.
(3) Use the total cross section to determine the probability of interaction for each neutron along the path length, and select a scattering position.
(4) Weight neutron interaction with the absorption probability and select the type of interaction (coherent or incoherent).
(5) Select the wavevector and energy transfer from the dynamic structure factor used as a probability distribution. Apply the detailed balance.
(6) Check whether selection rules can be solved. If they cannot, repeat (5).
(7) Iterate this procedure from step 1 to 6 until the neutron leaves the sample.

The *McStas Isotropic_Sqw* component implementation requires to provide the coherent and incoherent dynamical structure factor as two text files containing a matrix of $S(q,\omega)$ values on specified momentum and energy axes. Additionally, bound cross sections, temperature, density of material and molecular weight can be specified within the file headers, or given as individual parameters to the component. The sample geometry is described from a set of simple shapes (box, cylinder, sphere), or using a file containing a set of point coordinates to define a closed volume (which may for instance be obtained by scanning a real sample with a laser probe).

As the component is part of a full instrument description, the incoming neutron beam is obtained from *McStas* components upwards in the instrument description, which usually include a neutron source (pulsed or continuous) and neutron optics (guides, choppers, monochromators,...). Any sample container is treated just as the sample itself, i.e. as a material surrounding the sample to be studied. This implies the ability of the component to handle embedded geometries as well as multiple scattering between the container and the sample, which are both implemented in the component code and *McStas*. The results of the computation are obtained using detector components following the sample component position in the instrument simulation sequence such as banana shaped monitors recording time and angular histograms (tallies). Some of these monitors can be made sensitive to, e.g. only multiple scattering, or scattering taking place in the container. Each histogram is saved into a single text file. There is no assumption in the component *Isotropic_Sqw* regarding the following detector specifications (type, dimensions).

We shall now present an example of virtual experiment using this method, comparing simulated results with actual experiments.

3. A virtual experiment: liquid Rb on a time-of-flight spectrometer

All classes of instruments have been simulated with *McStas* and some of these are included as examples in the software [22]. To date, these simulations have used very simple models to describe samples, for example a vanadium-like constant incoherent scatterer, elastically scattering powders and a simple inelastic scatterer, but without multiple scattering.

In order to use the sample model presented above, prior knowledge of the dynamic structure factor $S(q,\omega)$ is required. Currently, there are three methods to obtain the dynamic structure factor (q,ω) matrix required for the sample simulation:

(1) Use an analytical $S(q,\omega)$ function to generate a matrix with a regular q and ω sampling. Results obviously depend on the analytical models used. This is one of the methods used in Discus [34] and MSCAT [35].
(2) Use previous experimental data, taking into account detector efficiencies, instrument contribution, sample absorption, empty cell and background subtraction. The resulting dynamical structure factor depends on the quality of the data analysis. Moreover, the extracted $S(q,\omega)$ should only be used to simulate experiments on half of its dynamical range (see comment in Section 2.1).
(3) Compute the dynamic structure factor of the sample from molecular dynamics (MD).

In order to demonstrate the efficiency of the simulation methodology presented above, we have searched for past experiment results published together with estimates of multiple scattering effects. The extensive experiments on *l*-Rb by Copley et al. [31,40] and Demmel et al. [41,42] give a complete dynamic structure factor data set, and additionally estimate the multiple scattering effects using MSCAT [35]. Moreover liquid rubidium is a simple alkali liquid which can be accurately simulated by means of classical [41,43] and *ab initio* molecular dynamics methods. We have thus chosen the published liquid rubidium dynamics measurements as a basis for the validation of our code. Complementary virtual experiment results on other materials will be published separately.

In the following, we have set up a simple model of an instrument built with a source, a liquid sample and a large detector.

3.1. Simulation details

The instrument model mimics the beam characteristics of the hybrid time-of-flight spectrometer built at the Argonne CP-5 reactor [44]. The neutron beam is extracted from a continuous thermal source ($T = 300$ K), collimated in a vacuum tube with width and height of 4 cm, and monochromatized to produce a $E_0 = 4.94$ and 33.0 meV incoming energy (we use here the same notation as in Copley paper, $E_0 = E_i$) with an energy resolution of $\Delta E = 0.24$ and 1.07 meV full-width at half maximum (FWHM) respectively. A Fermi Chopper creates a pulse of neutrons with triangular time distribution of 6.4 and 9.5 μs half width for $E_0 = 4.94$ and 33 meV incoming energy respectively. The beam hits the sample at 2.88 m after being monochromatized. The incoming neutron flux (i.e. the reactor power) at the sample position was adjusted to match the intensity measurements reported in [44] as 1.5×10^4 and 1.7×10^4 neutrons/s for $E_0 = 4.94$ and 33.0 meV incoming neutron energies respectively. An oscillating radial collimator is positioned around the sample chamber in order to remove most of the furnace aluminum scattering contribution. The detector bank, centered on the sample position, has a radius of 2.5 m, with 205 tubes of height 45 cm covering an angular range from 10° to 120°. Each detector tube is filled with an ^{3}He gas at 6 bars and a stopping gas. The whole detector produces an angle-time intensity histogram. The simulation model only considers a single neutron pulse, and thus neglects frame overlap. The γ-ray background from the neutron source is neglected, as well as scattering in air and helium gas.

The simulated liquid rubidium sample geometry is as described in [31]. Disks of height and diameter 1.68 cm are stacked, separated by an infinitely thin absorbing material. The cylindrical assembly is contained in an aluminum can of thickness 0.045 cm. The sample cell total height is larger than the beam size. The sample is placed in an aluminum evacuated tank of diameter 30 cm, thickness 2 mm. The aluminum container elastic coherent scattering is modelled [45] using measured structure form factors [46], with constant $S_{inc}(q) = 1$ incoherent contribution.

The rubidium sample structure and dynamics are extracted from a classical molecular dynamics (MD) simulation [30]. The inter-atomic interaction is described by the effective two-body potential of Kambayashi and Kahl [47,48], with a core radius parameter $r_c = 1.307$ Å. This simple potential has been validated for temperatures close to the *l*-Rb melting point $T_m = 312$ K. In this study, we have used 520 rubidium atoms with a number density $n = 0.010288$ atoms per Å^3. The system was first equilibrated at $T = 315$ K in the (N, V, T) ensemble, and trajectories were then recorded over 50,000 time steps of $\Delta t = 1$ fs in the (N, V, E) microcanonical ensemble. The sound velocity is obtained from the small-q phonon slope at about $c = 1300$ m/s and the diffusion coefficient is determined from the molecular dynamics as $D = 0.23$ Å^2/ps at $T = 315$ K, in agreement with [43].

From the molecular dynamics simulation trajectories, we calculate the liquid rubidium dynamic structure factor $S(q, \omega)$ describing the structural and dynamical behaviour of the sample. $S(q, \omega)$ is computed with the help of the *nMoldyn* package [49], which allows us to evaluate separately the coherent and incoherent parts of the dynamic structure factor. We then use that data as input for the *McStas* [22] virtual experiment, using the instrument described above.

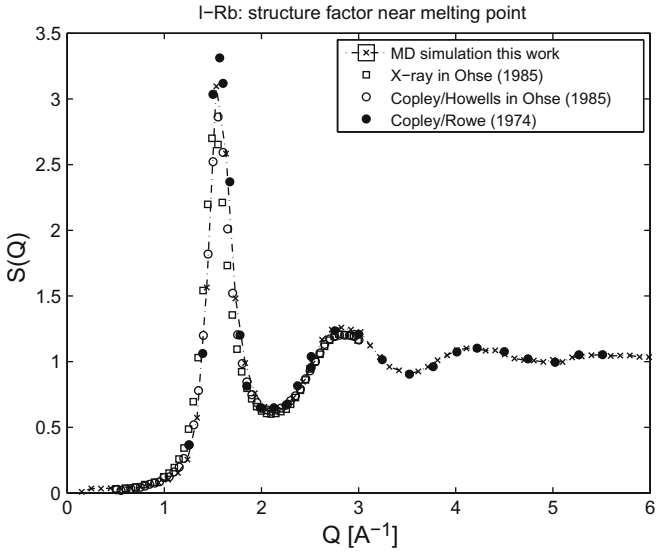

Fig. 1. Structure factor of *l*-Rb near the melting point: neutron scattering experiments [31,50] (circles), X-ray scattering [50] (squares) and MD simulation (crosses) at $T = 315$ K.

3.2. Results

In order to check the liquid rubidium molecular dynamics model, we first compare in Fig. 1 the static structure factor $S(q) = \int S(q,\omega)\,d\omega$ (where integration runs over the largest possible energy range) obtained from Copley measurements [31,50], X-ray data [50] and from our MD simulation. The simulated data are in good agreement with measurements, both in amplitude and phase. Around the first sharp peak at $q \sim 1.5$ Å simulation data is shifted to slightly lower q-values and is slightly sharper. This may originate from the limited size of the simulation box, which tends to slightly order the sample and thus show stronger structure peaks. As a consequence, we should expect in our simulation a stronger and sharper elastic peak contribution. These structure results are also in good agreement with those of Demmel [42]. This level of agreement is important to demonstrate since most of the multiple scattering events correspond to elastic scattering processes.

Copley [31] has measured the scattering function of liquid rubidium as a function of the time-of-flight and scattering angle. In order to determine the scattering function S from the measurement, the container and the instrument effects were subtracted and multiple scattering was estimated using MSCAT [35]. Such a data analysis procedure depends on the analytical and numerical models used.

In the current virtual experiment, the container and instrument are part of the simulation, and it is thus possible to produce raw data sets as if measured directly during the experiment, including the scattering from the sample as well as other contributions arising from the multiple scattering, the instrument geometry and the sample environment. In order to demonstrate how virtual experiments can produce results similar to the experimental ones, we have chosen to show the simulated raw time-of-flight data as a function of the angle, without any additional data analysis.

We have performed two simulations with incoming energies $E_0 = 4.94$ meV and $E_0 = 33$ meV. Each simulation generated 10^8 initial neutron events and ran for less than 15 min on a single processor machine. The simulation results correspond to

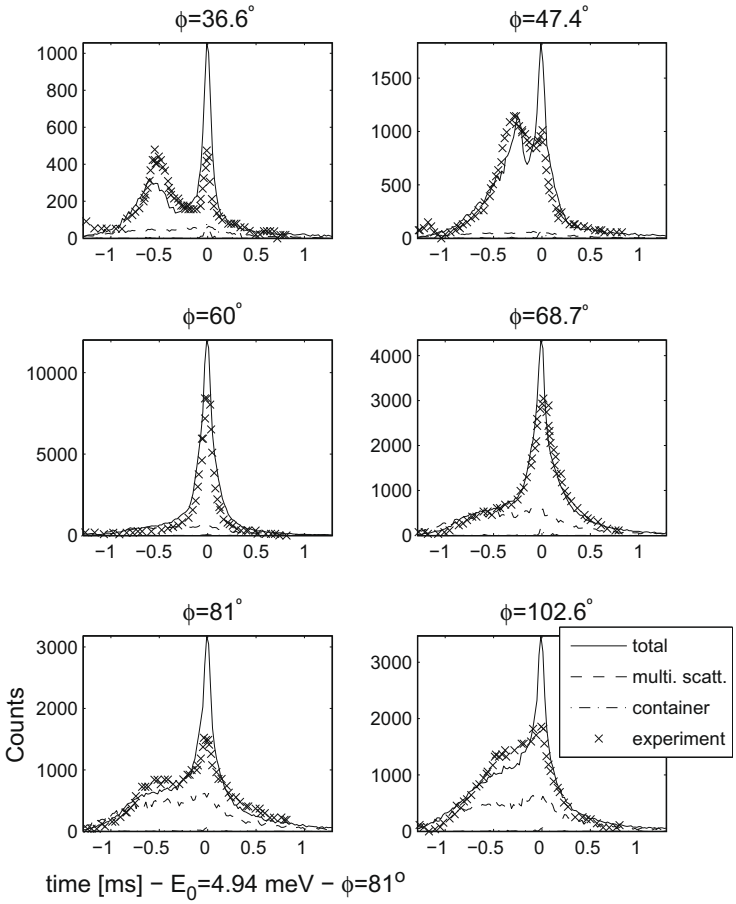

Fig. 2. *l*-Rb scattering (raw data) with incoming flux at $E_0 = 4.94$ meV showing the simulated total signal from sample (line) compared with the experimental data (crosses) from Ref. [31]. The sample environment (dash-dotted line, low intensity) and multiple scattering (dashed line) simulated contribution are also shown. The multiple scattering contribution has been multiplied by a factor 10, except for the two lowest angles. The corresponding wavevector transfer values for angles $\phi = 36.6°, 47.4°, 60°, 68.7°, 81°$ and $102.6°$ are $q = 1.06, 1.22, 1.37, 1.5, 1.68$ and $1.76\,\text{Å}^{-1}$ on the elastic line respectively.

an equivalent measurement time of the order of 40 h, but the corresponding experimental counting time is not indicated in [31]. Results of the virtual experiments using single detector tubes are shown in Figs. 2 and 3 and compared to time-of-flight experimental data from Ref. [31] at selected scattering angles.

It can be seen that both measurements and simulation show identical line shapes, with a sharper elastic line in the case of the simulation, as expected from the simulated structure factor (Fig. 1). Low angle results for $E_0 = 4.94$ meV incoming energy clearly present a distinct peak aside the elastic line. This peak, after transforming the time axis into energy transfer, reveals the liquid rubidium damped phonon in the case of the two lowest detection angles (see Fig. 4). However, this is not the case for the larger angles, in which case the apparent side peak does not correspond to any coherent single excitation, but originates from the time distribution transformation into energy bins, and disappears when extracting $S(q,\omega)$ [31]. The $E_0 = 33$ meV thermal incident energy results show a quasi-elastic line, slightly asymmetric.

The scattering from the sample container and the evacuated tank has also been simulated and appears as a central sharp peak, slightly displaced in time due to the cylindrical geometry. The multiple scattering contribution appears as a large quasi-elastic line which does not exceed a few percent of the total scattering. All contributions are obtained simultaneously, without additional scaling.

In order to compare our multiple scattering estimates with previous estimates like MSCAT [35], we have selected in Fig. 4 two representative plots of the scattering function at constant angle. The simulated data is obtained by changing the angle-time detector into an angle-energy transfer detector. This is achieved by storing at the sample position the energy transfer value, and access that information when neutrons reach the detector surface. There is no data analysis transformation and the result is obtained directly from the simulation, and not by treating the angle-time data as one would do from a real experiment. For the $E_0 = 4.94$ meV configuration, the lowest angle $\phi = 36.6^\circ$ shows the *l*-Rb phonon contribution, as well as the multiple scattering calculation. For the $E_0 = 33$ meV, we present results at scattering angle $\phi = 51^\circ$. As in the raw data, our simulated elastic line is sharper than the measured data. Both the scattering function and the multiple scattering contribution are in good agreement with the experiment and the MSCAT computation [31].

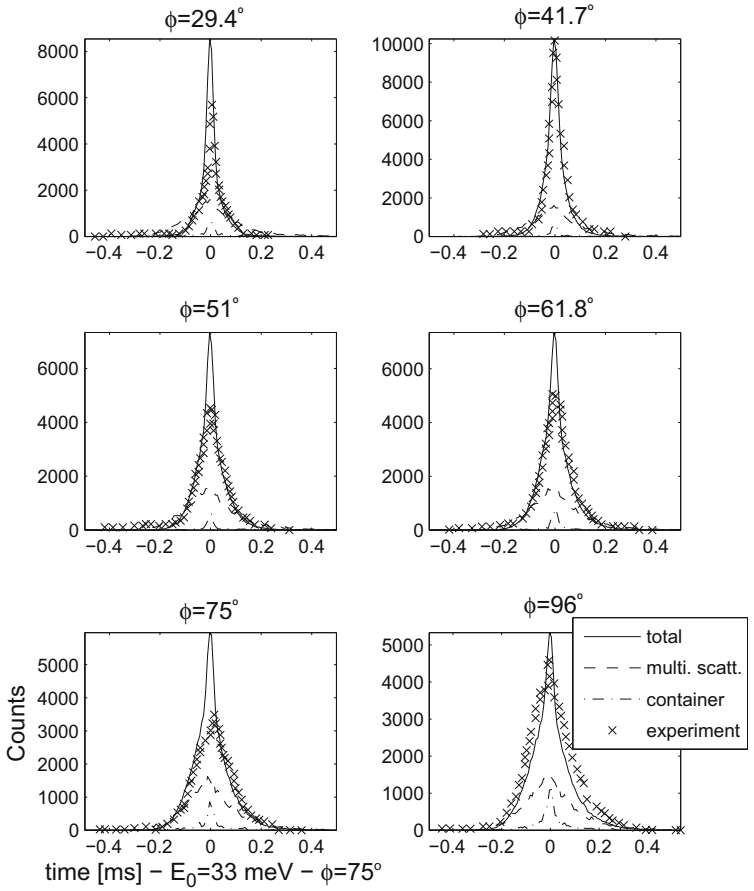

Fig. 3. *l*-Rb scattering (raw data) with incoming flux at $E_0 = 33$ meV showing the simulated total signal from sample (line) compared with the experimental data (crosses) from Ref. [31]. The sample environment (dash-dotted line) and multiple scattering (dashed line) simulated contribution are also shown. The multiple scattering contribution has been multiplied by a factor 10. The corresponding wavevector transfer values for angles $\phi = 29.4^\circ, 41.7^\circ, 51^\circ, 61.8^\circ, 75^\circ$, and 96° are $q = 2, 2.65, 3.1, 3.45, 3.76$, and $3.16\ \text{Å}^{-1}$ on the elastic line respectively.

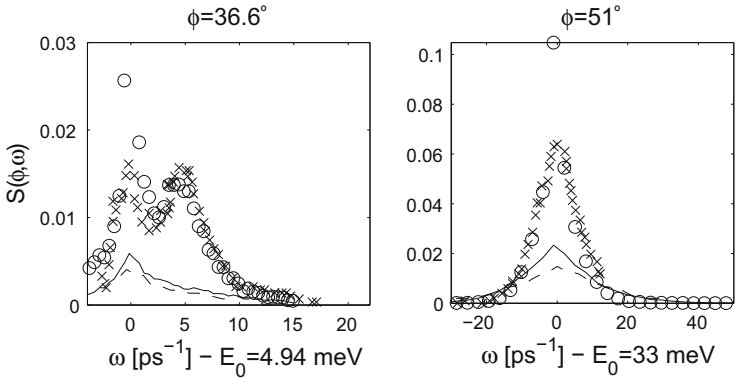

Fig. 4. *l*-Rb scattering function at constant angle with incoming flux $E_0 = 4.94$ meV (left) and $E_0 = 33$ meV (right) showing the simulated total signal from sample (circles) compared with the experimental data (crosses) from Ref. [31], and multiple scattering simulated in this work (line) and with MSCAT (dotted line). The corresponding wavevector transfer values for angles $\phi = 36.6°$ and 51° are $q = 1.06$ and 3.1 Å^{-1} on the elastic line respectively. The multiple scattering contribution is multiplied by a factor 10 for the $E_0 = 33$ meV configuration (right).

The sample is found to scatter 7.8% and 10% of the incoming intensity and the multiple scattering represents 5.4% and 4.8% of the scattering intensity at $E_0 = 4.94$ meV and $E_0 = 33$ meV incident energy respectively. The absorption fraction, including self-shielding, represents 11.1% and 4.5% at $E_0 = 4.94$ meV and $E_0 = 33$ meV incident energy respectively.

We thus conclude that within experimental and simulation uncertainty, the current virtual experiment is in good agreement with Ref. [31].

4. Discussion and perspectives

In this paper, we have presented a new method for the simulation of complete neutron scattering experiments, including both instrument and sample. The propagation of neutrons through the instrument and the sample uses Monte Carlo ray-tracing. For interactions between neutrons and the sample, the main kinds of processes are accounted for, such as absorption, coherent and incoherent scattering, and multiple scattering. The structural and dynamic features of the sample are described by its dynamic structure factor, which is used to compute the energy and momentum transfers between neutrons and sample. Sample environment elements are treated in the same way as the sample. This method generates a simulated signal of a neutron scattering experiment and gives insight into the influence of the different contributions to the experimental signal, which are otherwise difficult to evaluate accurately. In a usual neutron scattering measurement, the empty-cell contribution should be subtracted from the total signal, taking into account the relative absorption ratio between the cell and the sample itself on the cell geometry. The virtual experiment provides simultaneously in a single computation all contributions in the detected signal, with their absolute intensities (counts per second) and cross-scattering dependency. Specifically, the usual empty-cell measurement is not required to extract the sample-only contribution. This is especially relevant for materials with large absorption cross section, like indium and mercury.

Results of simulated neutron scattering experiments are shown for liquid Rb and compared to previous measurements. Despite the fact that our virtual experiment is somewhat simpler than the real experiment, simulated results are in very good agreement with experimental analysis. The simulation model was entirely computed, and results only depend on the two-body potential, its core radius parameter, the instrument geometry and the measurement time.

In the example presented here, the single scattering, dynamic structure factor is given as input in the virtual experiment and multiple scattering in the total signal is then evaluated. In the case of real experiments, only the total scattering is known and programs that treat multiple scattering attempt to extract the single scattering contribution. A logical extension to the approach developed here will therefore be to implement a self-consistent scheme in which the total signal is given as input, the multiple scattering is evaluated and then subtracted from the total to give new input signal and the cycle is repeated until the final, simulated total signal matches the initial, measured total signal. However, as stated before, this process can in principle only be applied on half of the measured dynamical range, so that the final input signal will approximate the single scattering, dynamic structure factor.

While treating multiple scattering only requires a simple model instrument, the numerical approach embodied in the virtual experiment allows complex instrument configurations. Since the sample component can be used to describe any scatterer, the virtual experiment can include any scattering elements that are in the incident beam or are likely to be irradiated by the scattered beam. Practically this type of simulation can be used to identify spurious contributions to the total signal, which may come from a series of scattering events in several elements, for example sample (elastic scattering)-cryostat (elastic scattering)-sample (inelastic scattering). While cryostats are generally not so problematic, cryomagnets and pressure cells can involve significant amounts of scattering materials close to the sample position. Such a sample environment may be

difficult to improve upon, but our simulations would allow the ideal beam characteristics to be determined for a given set of scattering elements around the sample position.

Finally, we intend to make virtual experiments available to new and established users of neutron scattering facilities in order to allow them to understand how experiments work and to evaluate if a proposed experiment is feasible. When some knowledge about the container and/or the sample is available, it is possible to compute accurately their contributions in a measurement, providing potentially, invaluable help in data analysis.

Acknowledgments

We gratefully thank J.R.D. Copley, H. Fischer, D. Champion, A. Filhol and J. Ollivier for helpful discussions. We would like to thank Professor G. Kahl for providing us with the code for computing the liquid rubidium potential used in the classical molecular dynamics simulations. All simulations were performed using the computing resources available at the ILL. *McStas* is supported as a JRA of the NMI3 network by the European Commission under the 6th Framework Programme through the Key Action: Strengthening the European Research Area, Research Infrastructures. Contract no.: RII3-CT-2003-505925.

References

[1] H. Maier-Leibnitz, T. Springer, Reactor Sci. Technol. 17 (1963) 217.
[2] D.F.R. Mildner, Nucl. Instrum. Methods Phys. Res. A 290 (1990) 189.
[3] R.A. Lowde, J. Nucl. Energy Part A: Reactor Sci. 11 (1960) 69.
[4] J.R.D. Copley, Nucl. Instrum. Methods Phys. Res. A 510 (2003) 318.
[5] E. Fermi, J. Marshall, L. Marshall, Phys. Rev. 72 (1947) 193.
[6] J. Peters, Nucl. Instrum. Methods Phys. Res. A 540 (2005) 419.
[7] C.D. Clark, E.W.J. Mitchell, D.W. Palmer, I.H. Wilson, J. Sci. Instrum. 43 (1966) 1.
[8] A.K. Freund, Nucl. Instrum. Methods Phys. Res. 213 (1983) 495.
[9] V.F. Sears, Acta Cryst. A 53 (1997) 35.
[10] G. Shirane, S.M. Shapiro, J.M. Tranquada, Neutron Scattering with a Triple-Axis Spectrometer, Cambridge University Press, 2002.
[11] L. Alianelli, J. Appl. Cryst. 37 (2004) 732.
[12] V. Radeka, IEEE Trans. Nucl. Sci. NS-21 (1974) 51.
[13] V. Peskov, G. Charpak, W. Dominik, F. Sauli, Nucl. Instrum. Methods A 277 (1989) 547.
[14] G. Manzin, B. Guerard, F.A.F. Fraga, L.M.S. Margato, Nucl. Instrum. Methods Phys. Res. A 535 (2004) 102.
[15] J.R.D. Copley, J. Neutron Res. 1 (1993) 21.
[16] L.D. Cussen, J. Appl. Cryst. 36 (2003) 1204.
[17] F. James, Rep. Prog. Phys. 43 (1980) 1145.
[18] J.R.D. Copley, P. Verkerk, A.A. van Well, H. Fredrikze, Comput. Phys. Commun. 40 (1986) 337.
[19] D.F.R. Mildner, C.A. Pellizari, J.M. Carpenter, Acta Cryst. A 33 (1977) 954.
[20] P.A. Seeger, L.L. Daemen, T.G. Thelliez, R.P. Hjelm, Phys. B 283 (2000) 433. <http://www.paseeger.com/>.
[21] J. Saroun, J. Kulda, Phys. B 234 (1997) 1102. <http://omega.ujf.cas.cz/restrax/>.
[22] P. Willendrup, E. Farhi, K. Lefmann, Phys. B 350 (2004) 735;
K. Lefmann, K. Nielsen, Neutron News 10 (1999) 20. <http://www.mcstas.org/>.
[23] D. Wechsler, G. Zsigmond, F. Streffer, F. Mezei, Neutron News 11 (2000) 25. <http://www.hmi.de/projects/ess/vitess/>.
[24] W.-T. Lee, X.-L. Wang, Neutron News 13 (2002) 30.
[25] E. Farhi, T. Hansen, A. Wildes, R. Ghosh, K. Lefmann, Appl. Phys. A 74 (2002) S1471.
[26] C. Schanzer, P. Boni, U. Filges, T. Hils, Nucl. Instrum. Methods Phys. Res. A 529 (2004) 63.
[27] G. Zsigmond, K. Lieutenant, S. Manoshin, H.N. Bordallo, J.D.M. Champion, J. Peters, J.M. Carpenter, F. Mezei, Nucl. Instrum. Methods Phys. Res. A 529 (2004) 218.
[28] K. Lieutenant, J. Phys.: Condens. Matter 17 (2005) S167.
[29] H. Schober, E. Farhi, F. Mezei, P. Allenspach, K. Andersen, P.M. Bentley, P. Christiansen, B. Cubitt, R.K. Heenan, J. Kulda, P. Langan, K. Lefmann, K. Lieutenant, M. Monkenbusch, P. Willendrup, J. Saroun, P. Tindemans, G. Zsigmond, Nucl. Instrum. Methods Phys. Res. A 589 (2008) 34.
[30] V. Hugouvieux, E. Farhi, M.R. Johnson, W. Kob, Phys. B 350 (2004) 151. See also V. Hugouvieux, A complete simulation of neutron scattering experiments, Ph.D. Manuscript, Univ. Montpellier, France, 2004.
[31] J.R.D. Copley, J.M. Rowe, Phys. Rev. A 9 (1974) 1656.
[32] V.F. Sears, Adv. Phys. 24 (1975) 1.
[33] F.G. Bischoff, M.L. Yeater, W.E. Moore, Nucl. Sci. Eng. 48 (1972) 266.
[34] M.W. Johnson, Harwell report, AERE – R 7682, March 1974.
[35] J.R.D. Copley, Comput. Phys. Commun. 7 (1974) 289.
[36] C. Petrillo, F. Sacchetti, Acta Cryst. A 46 (1990) 440;
C. Petrillo, F. Sacchetti, Acta Cryst. A 48 (1992) 508.
[37] G.L. Squires, Thermal Neutron Scattering, Cambridge University Press, 1978.
[38] V.F. Sears, Neutron News 3 (1992) 26.
[39] M. Matsumoto, T. Nishimura, ACM Trans. Model. Comput. Simul. 8 (1998) 3.
[40] J.R.D. Copley, J.M. Rowe, Phys. Rev. Lett. 32 (1974) 49.
[41] F. Demmel, A. Diepold, H. Aschauer, C. Morkel, J. Non-Cryst. Sol. 353 (2007) 3164.
[42] F. Demmel, D. Pasqualini, C. Morkel, Phys. Rev. B 74 (2006) 184207.
[43] J.-F. Wax, R. Albaki, J.-L. Bretonnet, Phys. Rev. B 65 (2001) 014301.
[44] R. Kleb, G.E. Ostrowski, D.L. Price, J.M. Rowe, Nucl. Instrum. Methods 106 (1973) 221.
[45] P. Willendrup, U. Filges, L. Keller, E. Farhi, K. Lefmann, Phys. B 386 (2006) 1032.
[46] P.H. Miller Jr., J.W.M. DuMond, Phys. Rev. 57 (1940) 198.
[47] S. Kambayashi, G. Kahl, Phys. Rev. A 46 (1992) 3255.
[48] G. Kahl, S. Kambayashi, J. Phys.: Condens. Matter 6 (1994) 10897.
[49] T. Rog, K. Murzyn, K. Hinsen, G.R. Kneller, J. Comput. Chem. 24 (2003) 657.
[50] W. Ohse, Handbook of Thermodynamic and Transport Properties of Alkali Metals, Ac. Press, Oxford, 1985.